PNAS RESEARCH ARTICLE | APPLIED PHYSICAL SCIENCES

A molecular interpretation of the toughness of multiple network elastomers at high temperature

Juliette Slootman[a], C. Joshua Yeh[a], Pierre Millereau[a], Jean Comtet[a,1], and Costantino Creton[a,1]

Edited by Steve Granick, Institute for Basic Science, Ulju-gun, Ulsan, South Korea; received September 1, 2021; accepted February 3, 2022

Unfilled elastomers often suffer from poor fracture resistance at high temperature where viscoelastic dissipation is low. A molecular design based on multiple interpenetrating networks composed of a brittle filler network isotropically prestretched to a value λ_0 by swelling it in an extensible matrix leads to a dramatic increase of fracture energy Γ_c, typically attributed to sacrificial bond scission creating a dissipative damage zone ahead of the propagating crack. However, the molecular mechanisms controlling the size of the damage zone when the crack propagates are currently unknown. Here, we combine fluorogenic mechanochemistry with quantitative confocal mapping and mechanical testing to characterize both Γ_c and the extent of bond scission in the sacrificial network detected on the fracture surfaces for different stretch rates and temperatures. We find that increasing the prestretch λ_0 of the filler network leads to a large increase in Γ_c mainly at temperatures well above the glass transition temperature of the elastomers, where viscoelasticity is inactive, but also at lower temperatures where both mechanisms are coupled. Yet, we show that there is no direct linear relation between the extent of filler network scission and Γ_c. We mainly attribute the large increase in Γ_c to the dilution of highly stretched strands in the entangled and unstretched matrix, which delocalizes stress upon bond scission and effectively protects the matrix network from scission and the material from crack growth. Delaying the localization of bond scission by network design is a promising strategy that will guide molecular designs able to toughen elastomers even in the absence of viscoelastic dissipation.

elastomer | mechanochemistry | fracture | fluorescence

Significance

Soft materials can be toughened by creating dissipative mechanisms in stretchy matrixes. Yet using them over a wide range of temperatures requires dissipative mechanisms independent of stretch rate or temperature. We show that sacrificial covalent bonds in multiple network elastomers are most useful in toughening elastomers at high temperature and act synergistically with viscoelasticity at lower temperature. We do not attribute this toughening mechanism only to the scission of bonds during crack propagation but propose that the highly stretched network diluted in a stretchy matrix acts by simultaneously stiffening the elastomer and delaying the localization of bond scission and the propagation of a crack. Such a toughening mechanism has never been proposed for elastomers and should guide network design.

Elastomers find numerous applications both in classical engineering and more recently in areas such as the biomedical field, wearable electronics, or soft robotics, where their flexibility and reversible elastic deformability are essential. Yet, it has long been known that they remain limited in their usage temperature by an intrinsic embrittlement as temperature increases well above their glass transition temperature (1, 2). This limitation has been investigated in detail with conventional unfilled elastomers and also with tougher grades filled with nanoparticles (3).

Indeed, while the incorporation of hard filler nanoparticles in the soft elastomer matrix leads to toughening, viscoelasticity still plays a major role in energy dissipation. The nanoparticles simply delocalize efficiently the regions that are exposed to high strain rates and high strains, create nanocavities (4), and generally enhance the strain seen by the elastomeric matrix. All of these mechanisms may still be present at temperatures well above the glass transition temperature of the elastomers (T_g). However, the lack of viscoelasticity of the matrix material at high temperature clearly reduces the stretch at break of the elastomer (3) so that, with the notable exception of strain-crystallizing filled natural rubber, all filled and unfilled elastomers suffer from a dramatic decrease in strength and toughness as the temperature is increased.

In 2003, Gong and coworkers (5) introduced a different strategy to toughen soft hydrogels, relying on the creation of an interpenetrating double network structure, where a brittle network (playing the role of the filler) is swollen and stretched in a ductile second network of polymer (the matrix). This molecular design strategy was later extended to elastomeric materials (6, 7), demonstrating the generality of the toughening mechanism due to multiple interpenetrating networks.

It is now well accepted that mechanical reinforcement in such multiple network gels or elastomers relies on the presence of sacrificial bonds embedded in the material (the stiff and brittle filler network) (8, 9). These sacrificial bonds break preferentially during crack propagation, leading to the presence of a damaged region extending toward the bulk of the material (6, 10–12). Tanaka (13) and Brown (12) attributed the toughening to the enhanced energy dissipation during the steady-state propagation of this local damaged region ahead of the crack tip. Experimental evidence for the existence of such extended damage at the crack tip (ranging from 100 μm up to few millimeters) has

Author affiliations: [a]Laboratoire SIMM, ESPCI Paris, PSL University, CNRS, Sorbonne Université, 75231 Cédex 05 Paris, France

Author contributions: J.S. and P.M. carried out the experiments; C.J.Y. and J.C. carried out the data analysis with help from J.S. and P.M.; C.C. planned the experiments and supervised the work; and J.C. and C.C. wrote the paper with input from all authors.

The authors declare no competing interest.

This article is a PNAS Direct Submission.

[1]To whom correspondence may be addressed. Email: costantino.creton@espci.psl.eu or jean.comtet@espci.psl.eu.

This article contains supporting information online at http://www.pnas.org/lookup/suppl/doi:10.1073/pnas.2116127119/-/DCSupplemental.

Published March 24, 2022.

been obtained for double network hydrogels by atomic force microscopy (AFM) (14), optical microscopy (11), and mechanochemistry (10), with some studies showing a correlation between the increase in fracture energy and the size of the damaged zone (6, 11). Similar qualitative observations were obtained for multiple network elastomers (MNE) by using mechanoluminescent probes (6) and fluorescent probes (15). However, the exact mechanisms accounting for the transfer of stress at the molecular scale between the filler network and the matrix and the role played by the filler network prestretch on material reinforcement remain to be clarified.

Reinforced soft materials, and MNE in particular, can be loaded over a wide range of strain rates and temperatures, begging the question of the role played by viscoelastic dissipation on the fracture process. In hydrogels, the few studies which probed a rate effect showed a weak dependence of fracture energy on crack velocity (16, 17). Concerning the effect of temperature on fracture energy, while an interesting study has been recently published to probe the toughness of salt-containing gels below freezing temperature (18), little has been done at temperatures higher than ambient for gels in part due to experimental difficulties in avoiding evaporation. Due to their viscoelasticity, fracture properties of filled and unfilled elastomers (without any solvent) can show a strong dependence on temperatures (19) and the results form the base of viscoelastic models of fracture (20, 21). However, how viscoelasticity couples with bond scission in reinforced multiple networks is currently not known.

Recently developed mechanophore strategies (6, 7) can act as a quantitative reporter for the level of bond scission in materials (22) and have the potential to illuminate those issues. Quantitative mechanochemistry has recently revealed that in simple elastomers, energy dissipated by bond scission occurs relatively far from the crack plane and contributes significantly to the fracture energy, while being closely coupled to the level of viscoelastic dissipation during crack propagation (22). In MNE, a large population of prestretched strands are introduced in the material. Upon stretching of the MNE, some of these strands will be overloaded at much lower values of macroscopic strain than the main bond population and lead to sacrificial bond scission (23, 24). Since, in the range of explored temperatures, the force to break a covalent bond is much less dependent on the temperature than viscoelastic friction, we could expect sacrificial bonds to act in a similar way, independent of temperature.

In this study, we probed the effect of strain rate and temperature on the fracture of MNE and investigated how the macroscopic fracture energy Γ_c couples with viscoelastic energy dissipation and sacrificial bond scission. We focused on simple and multiple network elastomers, where the filler network, synthesized first, was tagged with the damage-reporting anthracene-based cross-linking molecule. Fracture experiments carried out at various temperatures and stretch rates were combined with postmortem confocal microscopy observations of the fracture surfaces at room temperature, providing insights on the intrinsic couplings between network architecture, viscoelastic dissipation, and bond scission in reinforced soft matter.

Results

Preparation and Bulk Mechanical Properties of Multiple Network Elastomers. As shown in Fig. 1*A*, and previously described in more detail (7, 24), we synthetized multiple network elastomers based on poly(methyl-acrylate) (PMA) and poly(ethyl-acrylate) (PEA) through successive swelling and polymerization steps. We started by the synthesis of the sacrificial filler networks with a total cross-link density of 4×10^{25} m^{-3} to 5×10^{25} m^{-3} [extracted from the fit of the stress–strain curves and corresponding to an average of 320 to 370 C-C bonds per network chains; *SI Appendix*, section SI.3; Slootman et al. (22)]. In these networks, 5% of the cross-linkers are replaced by a mechanosensitive Diels Alder cross-linker (DACL), which becomes fluorescent upon scission and can thus operate as a quantitative reporter of chain damage (22). These networks are then swollen in a bath of methyl acrylate or ethyl acrylate monomers and cross-linker, which are subsequently polymerized at a much lower cross-link density of 0.01 mol% relative to monomer (typically, the monomer of the matrix and filler are the same). These swelling and polymerization steps can be repeated several times to obtain double and triple networks, respectively. As shown in *SI Appendix*, Fig. S2, the mechanical properties of labeled and unlabeled samples are identical within experimental error.

As proposed by Millereau et al. (7), it is interesting to compare these materials according to the prestretch λ_0 of the filler network, where we have $\lambda_0 = 1$ for single network elastomers (bare filler network) and typically $\lambda_0 \approx 1.6$ for double networks (one matrix swelling and polymerization step) and $\lambda_0 \approx 2.3$ for triple networks (two successive swelling steps). Fig. 1*B* shows representative stress-stretch curves of the model PMA materials in uniaxial extension with the three levels of filler prestretch. As shown in these stress/strain curves and described previously (7, 24), the network prestretch shifts the onset of strain hardening toward decreasing strains. If we rescale these curves by plotting the effective stress applied on the first network $\sigma_{FN} = \lambda_0^2 \sigma_N$ as a function of the effective strain seen by the filler network $\lambda_{FN} = \lambda_0 \lambda$, we observe a good collapse of the strain hardening part of the mechanical response of the three materials (Fig. 1*C* and *SI Appendix*, Fig. S3), demonstrating that the first network is effectively carrying most of the load in uniaxial extension in the nonlinear regime of the stress–stretch curve (7). Remarkably, under this normalization, it appears clearly that the average effective stretch at break of the filler network strands increases markedly depending on the prestretch, namely, to $\lambda_{FN} \approx 4$, 5.5, and 7.5 for single networks (SN), double networks (DN), and triple networks (TN) (see blue, red, and black vertical arrows), respectively. This result suggests that prestretching and diluting the filler network delays the onset of crack propagation. Note that no significant change in linear viscoelastic properties (*SI Appendix*, Fig. S4*C*) is measured for these three networks that share a nearly identical T_g.

Fracture Toughness of MNE at Various Temperatures. To probe in more detail how the structure of these materials affects their strength and their limiting extensibility, we propagate cracks in uniaxial extension in single-edge notched samples and extract the fracture energy Γ_c ($J.m^{-2}$) for each experimental condition by using Greensmith's approximation (22, 25) (*SI Appendix*, section SI.2). Stress–strain curves of these notched samples are shown in Fig. 2*A* for experiments carried out with PMA-based MNE at 25 °C (plain curves) and 80 °C (dashed curves). For identical initial notch lengths, Γ_c scales with the integral under the stress–stretch curve to fracture, and we clearly observe a large increase in Γ_c for increasing values of the prestretch λ_0 (comparing blue, red, and black mechanical curves). Note that although the critical stretch at break λ_c decreases with increasing prestretch, the critical stretch at break of the filler network λ_{FN}, which takes into account the filler network prestretch, increases (Fig. 1*C* and *SI Appendix*, Fig. S3).

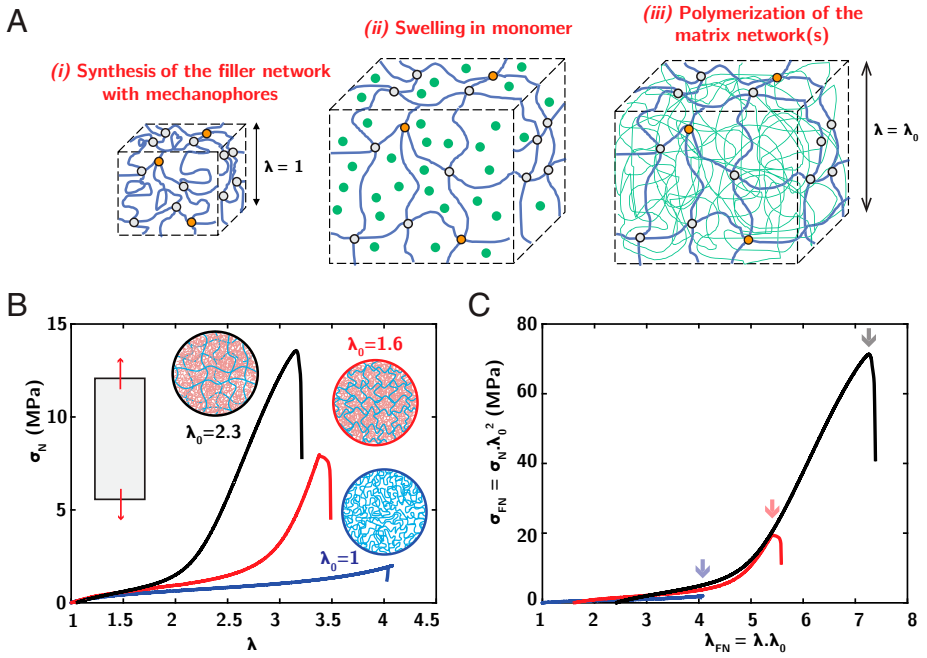

Fig. 1. Mechanics of MNE in uniaxial extension. (*A*) Synthesis of multiple network elastomers, with subsequent swelling and polymerization steps. The filler network is represented in blue and the matrix network in green. Orange cross-links represent mechanosensitive DACL cross-links. (*B*) Nominal stress σ_N as a function of strain λ for unnotched PMA multiple network elastomers, with three levels of network prestretch (blue, red, and black corresponding to $\lambda_0 = 1$, 1.6, and 2.3, respectively, i.e., simple, double, and triple network). (*C*) Normalized nominal stress $\sigma_{FN} = \sigma_N.\lambda_0^2$ carried out by the filler network as a function of the effective strain $\lambda_{FN} = \lambda\lambda_0$ seen by the filler network. Vertical arrows indicate the effective filler network strain at break.

When carrying out crack-propagation tests at various temperatures, we observe an increase in Γ_c with decreasing temperature (comparing plain and dashed curves, corresponding to temperatures of 25 °C and 80 °C) consistent with a more viscoelastic and dissipative character. However, Fig. 2*B* shows that while a higher temperature dramatically decreases Γ_c for single networks in agreement with previous work (1, 22), the effect is much less marked for the double networks ($\lambda_0 = 1.6$) and even more so for the highly prestretched triple networks ($\lambda_0 = 2.3$). Qualitatively, similar trends have been found over a larger range of temperatures for PEA-based materials (*SI Appendix*, Fig. S6).

To further analyze the macroscopic fracture behavior of these different network architectures, we report in Fig. 2*C* the fracture energy Γ_c as a function of the critical stretch at break of notched samples λ_c noting that all samples have nearly identical notch lengths of $\sim 0.9 \pm 0.25$ mm. We include in this plot the response of both PEA and PMA networks as circles and squares, respectively, where the PEA material has a lower glass transition temperature of −18 °C. Although these two networks have distinct glass transition temperatures and hence distinct viscoelastic properties in the range of temperatures probed here, we observe three families of curves for the various levels of prestretch. As expected, when increasing the degree of prestretch, the fracture energy Γ_c reaches larger absolute values at lower critical strain, due to network stiffening.

Following a similar idea as in Fig. 1*C* and ref. 7 regarding the composite nature of multiple networks, it is tempting to rescale Γ_c and λ_c accounting for the prestretch λ_0 of the filler network. We thus plot in Fig. 2*D* the evolution of $\Gamma_c\lambda_0^2/\Sigma_0$, the dissipated energy Γ_c per mole of filler network strands crossing the fracture plane, as a function of $\lambda_c\lambda_0$, the critical strain of the filler network at the onset of crack propagation. Physically, this is equivalent to considering the fracture energy per sacrificial network strand crossing the fracture plane as a function of the average stretch in the tensile direction of the filler network at the fracture point. Although experiments with different initial notch lengths would have given different values of λ_c, the point of this graph is the excellent collapse of the data in Fig. 2*D* in a single envelope for distinct material prestretches and glass transition temperatures. The existence of this master curve of the locus of fracture points is analogous to the fracture envelope proposed by Smith for simple network elastomers at different strain rates and temperatures (26). However, it is observed here to apply remarkably well to distinct materials, when considering the effective strain at break $\lambda_c\lambda_0$ and the fracture energy per network strand $\Gamma_c \cdot \lambda_0^2$ associated with the filler network. This global exponential rescaling characterizes the key role played by the filler network on the elastic properties of these materials and the highly nonlinear deformation response of the filler network.

Damage Quantification in Multiple Network Elastomers. In order to rationalize the large changes in toughness observed when varying network architecture and viscoelasticity, we take advantage of the mechanophores incorporated in the sacrificial filler network to quantitatively characterize the level of filler network damage following crack propagation. As schematically shown in Fig. 3*A*, when connected to a chain under tension, the mechanophore cross-linker can undergo a force-induced scission leading to the activation of its fluorescence. As reported in our previous work on simple network elastomers (22), the degree of mechanophore activation and fluorescence intensity in the sample following crack propagation can then be used to account representatively and quantitatively for the fraction of broken chains in the tagged network (here, the sacrificial filler network), when using a dilute concentration of mechanophore cross-links.

After propagating cracks in the material at different loading rates and temperatures for each material, we map postmortem the

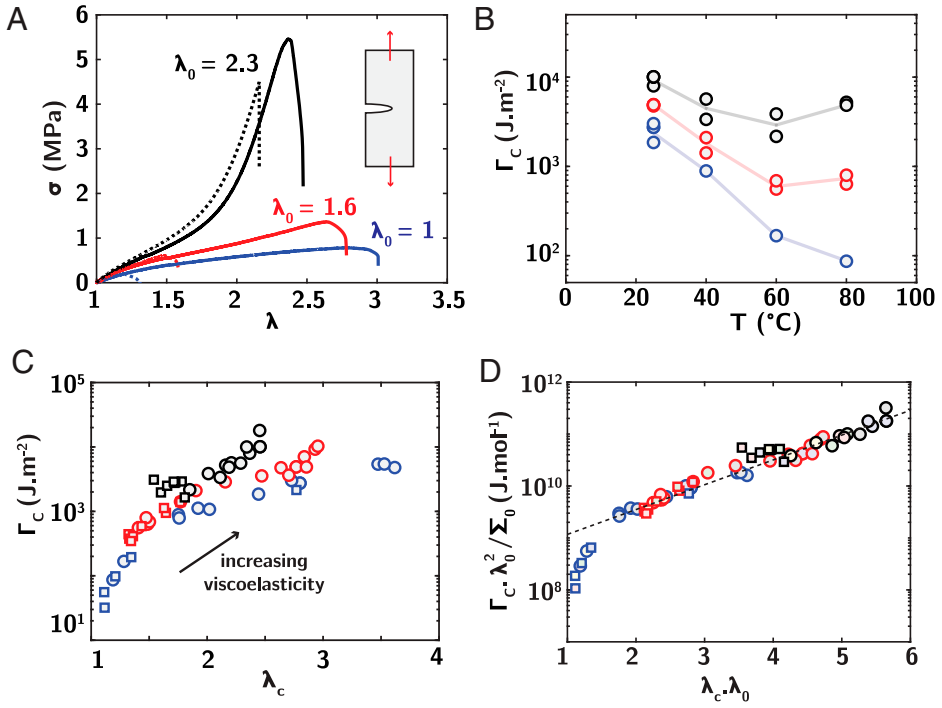

Fig. 2. Fracture toughness of multiple network elastomers. (*A*) Stress-stretch curves of notched samples of PMA elastomers with different degrees of filler network prestretch λ_0 and temperatures. Plain lines (25 °C) and dotted lines (80 °C), stretch rate of 3×10^{-3} s^{-1}. Blue, red, and black lines correspond to single ($\lambda_0 = 1$), double ($\lambda_0 = 1.6$), and triple networks ($\lambda_0 = 2.3$), respectively. (*B*) Variation of Γ_c with temperature (same color legend as in *A*). (*C*) Γ_c as a function of the critical stretch at break λ_c for notched samples of PMA-based (circles) and PEA-based (squares) networks (same color legend as in *A*). (*D*) Evolution of the fracture energy per mole of filler chains crossing the interface $\Gamma_c\lambda_0^2/\Sigma_0$ as a function of the effective filler network strain at break $\lambda_c\lambda_0$ for notched samples of PMA- and PEA-based MNE. Dashed line is an exponential fit for $\lambda_c\lambda_0 > 1.8$. The value of Σ_0 is taken as 1.8×10^{17} ch/m^2. Note that all notched samples have nearly identical notch lengths of $\sim 0.9 \pm 0.25$ mm.

fluorescence signal due to mechanophore activation postmortem along the propagation path of the crack by performing confocal microscopy scans normal to the crack surface (Fig. 3*C* and *SI Appendix*, section SI.5). These scans allow us to extract the spatial maps of mechanophore activation and filler network damage close to the crack edge, as shown in Fig. 3*C*. These damage maps are found to depend strongly on both the network architecture, characterized by the level of prestretch of the filler network (comparing $\lambda_0 = 1.6$ and $\lambda_0 = 2.3$), and on the viscoelasticity of the material at the given conditions (comparing fracture at an identical stretch rate of $\dot{\lambda} = 3 \times 10^{-3}$ s^{-1} at 25 °C and 80 °C). From Fig. 3*C*, we can already see that increasing the degree of prestretch of the filler network and increasing viscoelasticity—two factors leading to an increase in toughness Γ_c, see Fig. 2*A*—also lead to a net increase of the amount and spatial extension of bond scission in the filler network.

To quantitatively analyze the level of damage and bond scission, we extract as shown in Fig. 3*D* the spatial profile of the

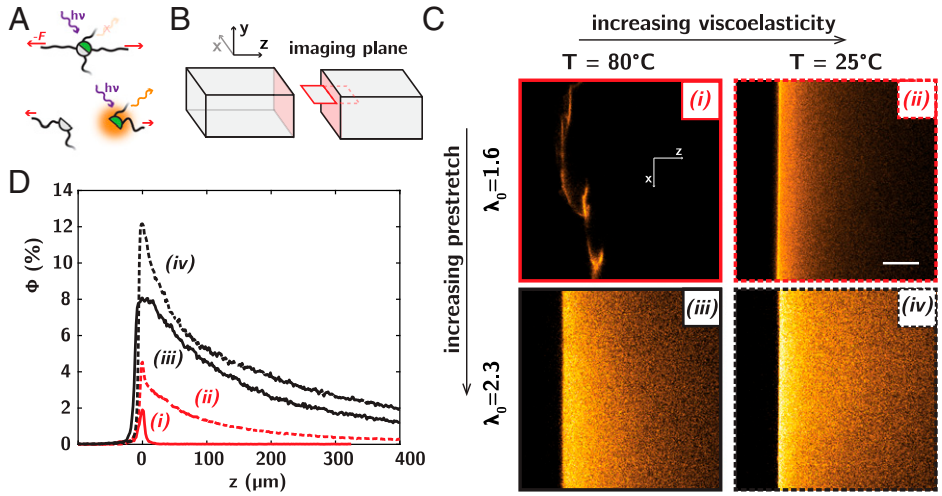

Fig. 3. Damage quantification in the filler network of the multiple network elastomers. (*A*) Schematic principle for chain damage detection through the scission-induced activation of the cross-linker mechanophore. (*B*) Schematic of confocal imaging plane in fractured samples. (*C*) Local intensity map due to mechanophore activation in PMA networks with increasing prestretch (*Top* to *Bottom*) and conditions of increasing viscoelasticity (80 °C and 25 °C, *Left* to *Right,* respectively). Plain and dashed red lines correspond to double networks ($\lambda_0 = 1.6$) at 80 °C and 25 °C. Plain and dashed black lines correspond to triple networks ($\lambda_0 = 2.3$) at 80 °C and 25 °C. The two materials are rendered with distinct intensity scales. (Scale bar, 100 μm.) (*D*) Damage profile ϕ normal to the crack edge, for the four conditions in *C*.

Table 1. List of analyzed and synthetized samples*

Sample name	λ_0	Monomer in filler network	Monomer in matrix and Tg (°C)	Areal density of chains, Σ_{LT}	Symbol	Elastic moduli
SN.EA	1	EA	EA (−18 °C)	1.8×10^{17} m^{-2}	■	1 MPa
SN.MA	1	MA	MA (18 °C)	1.9×10^{17} m^{-2}	○	1.15 MPa
DN.EA.EA	1.6	EA	EA (−18 °C)	6.7×10^{16} m^{-2}	■	1.3 MPa
DN.MA.MA	1.6	MA	MA (18 °C)	7.7×10^{16} m^{-2}	○	1.9 MPa
DN.MA.EA	1.5	MA	EA (−18 °C)	8.9×10^{16} m^{-2}	○	1.2 MPa
TN.EA.EA	2.3	EA	EA (−18 °C)	3.1×10^{16} m^{-2}	■	1.7 MPa
TN.MA.MA	2.3	MA	MA (18 °C)	3.6×10^{16} m^{-2}	○	2.2 MPa

*EA, ethyl(acrylate); MA, methyl(acrylate).

local damage $\phi(z)$ in the sacrificial network for increasing distances z from the crack plane. We define here ϕ as the local fraction of broken chains in the filler network, measured directly from the level of mechanophore activation (*SI Appendix*, section SI.5, details the measurement and quantification method). While damage appears very localized in the double network at high temperature (condition *i*), it progressively delocalizes over larger distances from the fracture plane and the overall quantity of broken bonds increases for conditions of increasing viscoelasticity (comparing *i* and *ii*) and increasing prestretch (comparing *i* and *iii*).

Interestingly, we find under all conditions a relatively smooth and progressive decay of local damage with distance from the crack surface. These measurements are distinct from the observation of a well-defined local damage zone with sharp boundaries at the crack tip, as reported in an earlier study on double network hydrogels (11). Under some conditions of large viscoelasticity and large prestretch (e.g., in triple networks of PMA at 25 °C; *SI Appendix*, Fig. S8), we further observe a bulk level of damage in the material [i.e., $\phi(z \to \infty) \to \phi_{bulk} \neq 0$). This bulk activation can reach up to $\phi_{bulk} \approx 3\%$ and correlates well with the macroscopic stretch at break. This observation suggests that bulk activation occurs under conditions where the effective stretch on the network chains in the bulk reaches their limiting extensibility upon material failure (*Discussion*). The appearance of the fracture surface is also dependent on fracture conditions and position along the fracture length. Most materials show a relatively smooth fracture surface, but rough fracture surfaces can also appear in conditions associated with low viscoelasticity and intermediate prestretch (e.g., Fig. 3 *C*, *i* and *SI Appendix*, Fig. S9).

We now compare these damage results with those of fracture energy Γ_c (J·m^{-2}). As we previously proposed (22), it is instructive to extract Σ (strands·m^{-2}), an integrated interfacial quantity characterizing the density of broken strands per unit surface of crack. This quantity can be simply extracted by summing the local damage inside the material along a unit area, as $\Sigma = 2\nu_x \int \phi(z) dz$ where ν_x (m^{-3}) is the density of polymer strands per unit volume of filler network initially present. This quantity can be defined for both smooth and rough profiles of the fracture surface (*SI Appendix*, Fig. S9). Under conditions where bulk damage is present, Σ is defined as the excess of chain scission at the crack tip $\Sigma = 2\nu_x \int [\phi(z) - \phi_{bulk}) dz$. Interestingly, spatial variations in the level of local damage of the filler network are observed over millimetric distances along the crack path in all samples, with sacrificial bond scission being systematically smaller close to the initial notch and larger on the opposite side of the sample. We obtain for the four samples reported here an average value of Σ near the fracture surface of $\Sigma_{(i)} = 7.4 \times 10^{18}$, $\Sigma_{(ii)} = 8.3 \times 10^{19}$, $\Sigma_{(iii)} = 1.7 \times 10^{20}$, and $\Sigma_{(iv)} = 2.7 \times 10^{20}$ strands·m^{-2}.

As we previously proposed (22), it is instructive and convenient to normalize this areal damage Σ by Σ_{LT}, the areal density of sacrificial network strands crossing a plane in the material. The ratio Σ/Σ_{LT} accordingly represents the additional density of broken sacrificial strands compared to the limiting situation where crack propagation would lead to broken strands along a single material mesh size. For unswollen single networks ($\lambda_0 = 1$), Σ_{LT} can be estimated as $\Sigma_{LT}^{SN} = 1/2 \cdot \nu_x < R_0^2 >^{1/2}$, with ν_x the volume density of cross-linking points and $< R_0^2 >^{1/2}$ the average distance between cross-links, expressed as a function of the network parameters (7) (*SI Appendix*, section SI.3). For swollen multiple networks, Σ_{LT} is reduced by the areal dilution factor due to network prestretch and expressed as $\Sigma_{LT} = \Sigma_{LT}^{SN}/\lambda_0^2$. We find values of Σ_{LT} of the order of 2×10^{17}, 8×10^{16}, and 2×10^{16} strands·m^{-2} for single, double, and triple networks, respectively (Table 1). Under the four conditions of Fig. 3, we thus obtain $\Sigma_i/\Sigma_{LT} \approx 95$, $\Sigma_{ii}/\Sigma_{LT} \approx 1{,}000$, $\Sigma_{iii}/\Sigma_{LT} \approx 4{,}800$, and $\Sigma_{iv}/\Sigma_{LT} \approx 7{,}600$. These results also provide an estimate of the width of the zone where sacrificial bonds break in units of mesh size and show that the length over which sacrificial bonds break when the crack propagates is of the order of hundreds of microns, a surprising result that will be discussed later. The results shown on Fig. 3*C* also clearly show that the extent of sacrificial bond scission is affected both by the network architecture (degree of prestretch λ_0) and by the viscoelastic effects (due to stretch rate).

Coupling between Damage, Fracture Energy, and Viscoelasticity. The methodology and analysis described above have been carried out for a range of strain rates and temperatures, and values of Γ_c and of Σ/Σ_{LT} have been measured for each condition. Following the methodology proposed in our previous work and detailed in the *SI Appendix* SI.3 and *SI Appendix*, Fig. S4, we assumed that time-temperature superposition can legitimately be used here. We first plot in Fig. 4*A* the evolution of the fracture energy Γ_c as a function of a rescaled crack velocity $a_T \cdot v_{crack}$. The average crack propagation velocity v_{crack} is extracted from the stress/strain curves and rescaled here by a time–temperature superposition factor a_T This factor characterizes matrix viscoelasticity through the temperature difference between the temperature at which the fracture test was carried out and the glass transition temperature of the matrix network. Indeed, PMA and PEA materials have distinct glass transition temperatures T_g of 18 °C and −18 °C, respectively, leading to distinct viscoelastic behavior at room temperature and above. The use of this rescaled crack velocity allows us to compare elastomers made from these two monomers and access a large

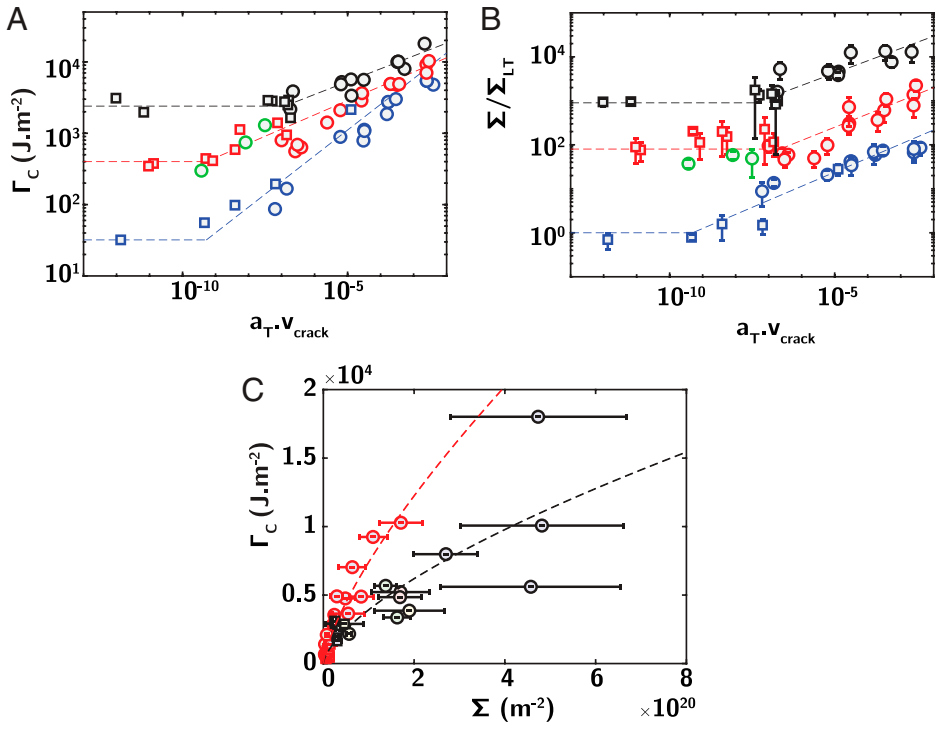

Fig. 4. Rate effects in fracture energy and damage activation in PMA and PEA network. Fracture energy (*A*) and normalized damage Σ/Σ_{LT} (*B*) as a function of rescaled crack propagation velocity $a_T \cdot v_{crack}$ for EA (square) and MA (circle); SN (blue) DN (red), and TN (black) networks; and the mixed double network DN.MA.EA (green). We observe a threshold in Γ_c and Σ/Σ_{LT} for low $a_T v_{crack}$. For large crack propagation velocity, the fracture energy and areal damage can be well approximated by a power-law scaling $\Gamma_c \sim (a_T \cdot v_{crack})^{\alpha}$ and $\Sigma/\Sigma_{LT} \sim (a_T \cdot v_{crack})^{\beta}$, with $\alpha = [0.36; 0.2; 0.18]$ and $\beta = [0.32; 0.3; 0.28]$, respectively, for increasing prestretch $\lambda_0 = [1; 1.6; 2.3]$. (*C*) Variation of the fracture energy Γ_c as a function of the total areal density of broken sacrificial bonds Σ for DN (red circles) and TN (black circles). The dashed lines are power-law fits $\Gamma_c \sim \Sigma^{\gamma}$, with $\gamma = 0.66$ and $\gamma = 0.73$ for DN and TN, respectively.

range of viscoelastic conditions (*SI Appendix*, Fig. S4). It is important to note that even during steady-state crack propagation the strain rate varies spatially and the average crack velocity characterizes here the range of strain rates that material points near the fracture surface have experienced during the propagation of the crack (21, 27, 28).

Remarkably, using this rescaled crack velocity allows us to successfully collapse the fracture energy (Fig. 4*A*) of materials possessing a similar architecture (given by the filler network prestretch, in blue, red, and black) but fractured at distinct temperatures and composed of distinct matrix monomers (squares and circles for EA and MA). The success of this rescaling, even for a mixed material composed of a minority PMA filler and a majority PEA matrix (green), shows that the viscoelastic properties of the matrix (used for the rescaling) contribute strongly to the observed toughening.

For each material with a given prestretch $\lambda_0 = 1$, 1.6, and 2.3, we can thus express phenomenologically the fracture energy as $\Gamma_c^{\lambda_0} \approx \Gamma_c^{\lambda_0,*} \cdot [1 + f_{\lambda_0}(a_\Gamma v_{crack})]$ with $\Gamma_c^{\lambda_0,*}$, a threshold fracture energy for conditions of low viscoelasticity, and f_{λ_0}, a function of the reduced crack velocity $a_\Gamma v_{crack}$ characterizing the evolution of the fracture energy for large viscoelastic dissipation. Importantly, and consistent with Fig. 2, we observe a strong increase in the threshold fracture energy $\Gamma_c^{\lambda_0,*}$ when increasing the network prestretch, with $\Gamma_c^{\lambda_0,*}$ reaching 30 J·m^{-2}, 400 J·m^{-2}, and 2,400 J·m^{-2} for single, double, and triple networks, respectively, (horizontal dashed lines). In viscoelastic conditions, the fracture energy is well approximated by a power-law behavior, $\Gamma_c \sim (a_\Gamma \cdot v_{crack})^{\alpha}$ (oblique dashed lines). Although the general evolution of Γ_c with $a_\Gamma . v_{crack}$ is the same, the absolute values of Γ_c are very different for the three classes of materials and the power-law exponent α, which characterizes the sensitivity of the material to viscoelastic dissipation decreases with increasing prestretch.

In summary, a larger prestretch leads to both a large increase in threshold fracture energy when viscoelastic dissipation is low and to a weaker sensitivity to viscoelastic dissipation. Since for these elastomers low viscoelasticity requires a high temperature, we find that the multiple network architecture is the most effective relative to conventional elastomers ($\lambda_0 = 1$) at high temperature.

Discussion

Coupling of Network Damage and Fracture Energy. To rationalize the remarkable performance of the multiple network architecture in conditions of low viscoelasticity at high temperature, we turn to the analysis of bond scission in these materials. As mentioned above, when plotting the areal density of bond scission $\bar{\Sigma} = \Sigma/\Sigma_{LT}$ as a function of $a_\Gamma . v_{crack}$, we observe qualitatively similar trends in the evolution of the damage, with a threshold value at low crack velocity, which increases for increasing prestretch (Fig. 4*B*, horizontal dashed lines) and a power-law increase at larger crack speed for increasing viscoelasticity (Fig. 4*B*, oblique dashed lines).

Given these similar trends, it is tempting to try to directly correlate the measured fracture energy with the areal density of broken sacrificial bonds Σ, as shown in Fig. 4*C*. If a Lake and Thomas argument holds for the energy dissipated per broken strand (29) and this is the only dissipative mechanism during crack propagation, one would expect a linear relation between Γ_c and Σ. Yet, although both quantities appear qualitatively correlated, we fail to see a linear relation independent of viscoelasticity and material's degree of prestretch. Over this linear

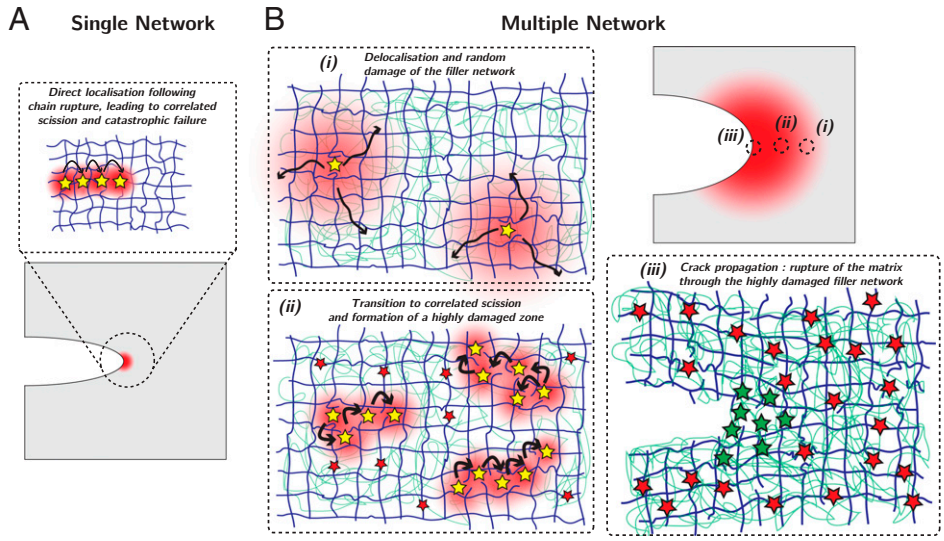

Fig. 5. Onset of crack propagation in MNE. The pictured mechanisms are at play under threshold conditions (no viscoelastic dissipation). (*A*) In a single network, chain rupture (yellow stars) leads to direct localization of the stress to the neighboring chains (red area), leading to correlated scission of adjacent chains (black arrows and yellow stars) and propagation of a localized crack. (*B*) In MNE, the failure mechanism is completely different. (*i*) Following chain rupture of the dilute filler network (yellow stars), stress is delocalized over a large area (red area and black arrows), through interactions between the filler network and the entangled matrix. Far away from the crack tip, this delocalization mechanism allows for random damage in the first network, with no interaction between chain scission events. (*ii*) Closer to the crack tip, bond scission starts to occur in a correlated fashion (smaller red area and black arrows), leading to the creation of an extended damage zone, with holes in the filler network and transfer of stress to the matrix. (*iii*) At the tip of this zone, the crack propagates through localized failure of this softened zone. Red stars represent the presence of damage in the filler network. Green stars characterize the localized rupture of the matrix network.

scale, the fracture energy is found to increase instead sublinearly with the areal density of broken bonds, as $\Gamma_c \sim \Sigma^{\gamma}$, with $\gamma \approx 0.6 - 0.7$. These observations call for a more refined interpretation of the couplings between bond scission and fracture energy.

Threshold bond scission at high temperature. To rationalize the increase in the threshold fracture energy $\Gamma_c^{\lambda_0,*}$ with increasing prestretch λ_0, we first focus on the observation in Fig. 4 *A* and *B* of a threshold level of sacrificial bond scission $\frac{\Sigma}{\Sigma_{LT}}$ at low viscoelasticity, which increases strongly when increasing the prestretch, from $\Sigma \approx \Sigma_{LT}^{SN}$ for $\lambda_0 = 1$, to $\Sigma \approx 10^2 \cdot \Sigma_{LT}^{DN}$ for $\lambda_0 \sim 1.6$, and up to $\Sigma \approx 10^3 \cdot \Sigma_{LT}^{TN}$ for $\lambda_0 \sim 2.3$. The increase in threshold damage accordingly implies that in the absence of additional dissipation mechanisms such as viscoelasticity, the threshold number of layers of broken bonds necessary for the crack to propagate increases strongly when diluting the filler network, i.e., bonds break much further away from the fracture plane. Even in absolute terms, Σ increases by a factor of 200 between SN and TN.

Understanding this effect of the molecular architecture on crack propagation is nontrivial. Considering the highly disordered nature of the filler network, the propagation of a macroscopic fracture in this material amounts to the nucleation of a localized percolating damage pathway. The increase in the total damage necessary for the crack to propagate would thus imply a delayed nucleation of this percolating pathway. Since no or little viscoelastic dissipation is present under these conditions, the corresponding mechanism must depend on the local architecture of the material and on the redistribution of stress upon chain scission.

It is first instructive to examine statistical models of failure in disordered networks, such as the so-called fiber bundle models (30), which provide an analogy with the disordered structure of the random filler network. A key parameter describing failure in these random networks is the redistribution of load following the rupture of a single strand (or fiber). In the first limit of local load sharing, the load following a rupture event is mainly redistributed to the neighboring strands, which leads to a rapid localization of damage through avalanches and ultimately failure (Fig. 5*A*). In the opposite limit of equal load sharing, all of the intact strands share equally the load of a broken strand, delaying localization of damage and macroscopic failure (Fig. 5 *B*, *i*). These limits correspond to extremes with respect to the spatial correlations in stress redistributions, and it is possible to interpolate in between to account for elastic correlations following a rupture event (31), leading accordingly to a transition between the critical and the mean-field behavior or, in other words, between correlated and random bond scission.

Based on these general concepts, we can now describe in more detail our vision of the role played by the network structure in delaying crack nucleation in MNE. In a single network, as shown schematically in Fig. 5*A*, the presence of a crack leads to stress concentration at the crack tip. Under threshold conditions, the load following a scission event is probably redistributed to the very neighboring strands, and bonds fracture in a correlated and localized way very close to the fracture surface (22), in qualitative agreement with the Lake and Thomas model (32).

As pictured in Fig. 5*B*, the mechanism of failure we propose for MNE is completely different. Far from the tip (regime *i*), bond scission occurs randomly in the filler network for the shorter and more highly stretched strands; upon scission of a single highly stretched strand, the load is redistributed by entangled matrix chains over an extended volume of matrix and filler network (depending on dilution) and not simply on the neighboring filler network strand (in the spirit of the equal load sharing scheme described above). The matrix network(s) must play a major role in this delocalization mechanism. Indeed, as demonstrated by Millereau et al. (7), the reinforcement is not observed when the matrix network(s) is replaced by oligomers or solvent or when the volume fraction of filler network is too high. The presence of the unstretched and entangled matrix is thus essential to carry and redistribute the

load upon scission of a sacrificial bond, and this stress transfer further away from the broken bond can only work if the filler is dilute and the matrix is unstretched or weakly stretched. In this regime, bond scission can be described by a mean-field model as proposed by Lavoie et al. (33) and Bacca et al. (34) in their damage models where the stretch relative to the undeformed state of the MNE must be the same for all networks. Hence, the probability of strand scission only depends on $\lambda_0\lambda$. *SI Appendix*, Fig. S3 *B* and *D* show that the bulk value of $\lambda_0\lambda$ at propagation increases significantly with prestretch, and if the strain fields around the crack tip are similar, regime *i* will extend much further from the tip of the crack as λ_0 increases.

Closer to the tip two other mechanisms become active. At some distance from the tip, the failure of the filler network bonds becomes correlated, causing the opening of large holes and extensive transfer of stress to the matrix with a pronounced softening (domain *ii* of Fig. 5*B*). The existence of this large-scale stress transfer mechanism from filler network to matrix network close to the crack tip for high values of λ_0 has recently been demonstrated for elastomers (15) and is well-documented for gels (10, 11, 14). Depending on boundary conditions, this softening can lead to an increase in stretch in the damaged zone which greatly increases the energy dissipated per broken bond (7). The formation of this softened damage zone is due to a transition from a mean-field situation where the probability of scission of a given strand is uniquely dependent on the stretch experienced by that strand to a correlated scission of filler network bonds where the probability of scission of a given strand is dependent on whether adjacent strands are broken or not. Such a non–mean-field scission presumably leads to the formation of larger-scale holes and cracks in MNE. It appears reasonable to assume that this transition from mean-field scission to correlated scission occurs above a certain value of stretch of the filler network $\lambda\lambda_0$. Hence, the more the filler network is prestretched, the lower the value of macroscopic experimental stretch where this transition can occur.

Finally, the steady state propagation of the crack requires the localized failure of this softened zone as shown in scheme *iii* of Fig. 5*B*. Regarding this final step, the hypothesis made by Brown (12) is that the crack will propagate when the strain energy stored in the damaged zone is sufficiently large to create a stress concentration at the tip of the crack (green stars in scheme *iii* of Fig. 5*B*), which is able to break the bonds of the damaged network (matrix and filler networks) (12). This hypothesis of failure due to a stress concentration in the highly damaged zone [inspired by the failure criterion of a plastic zone in a glassy polymer (35, 36)] is difficult for us to verify directly since we do not have access to the local strain energy or exact size of the highly damaged zone. However, the threshold values reported on Fig. 4 *A* and *B* suggest that the criterion of propagation is not directly proportional to the total areal density of broken sacrificial bonds (*SI Appendix*, Fig. S10). This propagation criteria must be more complex, involving other dissipative or damage mechanisms very close to the crack plane, as described above. The difference between DN and TN suggests that filler network scission in DN is more efficient at dissipating energy than in the TN. Such complex multiscale bond scission mechanisms are in principle only strain dependent and inherently strain rate independent. In the absence of viscoelasticity slowing down the crack (threshold conditions), they would result in a fast propagation, once the criterion of propagation outlined above is met.

While mechanism *iii* has to be by definition very localized and requires the failure of both filler and matrix strands, regime *ii* and *i* only involve the failure of the filler network. Our mechanochemistry data show that, at the propagation point, damage occurs over a larger and larger volume as the degree of prestretch of the filler network and the stretch rate increase (Figs. 4*B* and 5*B*). This is a key result of our investigation showing that the complex process of delay in correlated bond scission and transfer of the stress to the matrix is able to create a much larger damage zone before the crack can propagate. We can interpret this effect as an interplay between mean-field scission far from the tip, creating a large damage zone for large λ_0 (regime *i*) and delayed propagation of the crack through a highly damaged zone, where the stress is transferred to the matrix (regime *ii* and *iii*). Because of the complexity of the multiscale process, predicting the onset of regime *ii* and of regime *iii* at the crack tip as a function of λ_0 remains a challenge and requires a molecular criterion related to the network architecture. Recent simulation studies may provide hints on the nature of such criteria (37, 38).

Coupling of sacrificial bond scission with viscoelasticity and macroscopic deformation. We can now address the role played by viscoelasticity in the increase in fracture energy Γ_c and its coupling to sacrificial bond scission. For single networks ($\lambda_0 = 1$), viscoelastic dissipation can couple to bond scission through macroscopic strains at the crack tip (22). To probe more closely this coupling in this series of MNE, we plot in Fig. 6*A* the evolution of the areal density of broken chains Σ as a function of the macroscopic strain at break λ_c for notched samples having all the same initial notch length. For a given material and notch length, Σ increases with λ_c, i.e., with increasing viscoelasticity, and for a given λ_c, Σ increases with increasing prestretch (comparing blue, red and black points). Interestingly, focusing on the result of the double network (red points), sacrificial bond scission appears first independent of λ_c and then clearly increases for $\lambda_c > 2$.

It is then interesting to rescale the data, following similar ideas motivating Fig. 2*D*, by plotting in Fig. 6*B* the areal density of broken sacrificial bonds Σ, as a function of $\lambda_0\lambda_c$, the effective stretch of the filler network when the crack propagates. This normalization leads to a clear collapse of the data for the three levels of prestretch, from which we can identify three successive regimes. In regime 1, only observed for $\lambda_0 = 1$, viscoelasticity is coupled with localized bond scission and controls the crack tip stretch.

In regime 2 mainly observed for $\lambda_0 = 1.6$ far from T_g, Γ_c increases (Fig. 2*D*) but Σ stays constant (Fig. 6*B*). Viscoelastic dissipation is weakly coupled to bond scission, with $\Sigma \approx cst \approx 8 \times 10^{18}$ strands·m^{-2} controlled by the complex mechanism described above (Fig. 5) and viscoelasticity acting as an additive dissipative mechanism without much influence on the crack tip strains.

Regime 3 kicks in when the filler network chains become highly stretched, for which we observe a strong exponential coupling with macroscopic deformation with $\Sigma \sim \cdot e^{\alpha \cdot \lambda_c \lambda_0}$ for $\lambda_c\lambda_0 > 3.2$, with $\alpha = 1.75$. The upper axis shows the same data as a function of $\lambda_0\lambda_c/\lambda_{max}$, the effective strain normalized by the average limiting extensibility of the sacrificial chains $\lambda_{max} \sim 5.1$ (*SI Appendix*). The observed transition between these two regimes occurs for $\lambda_c\lambda_0 \sim 0.6 \cdot \lambda_{max}$, suggesting that this change of regime in sacrificial bond scission occurs when filler network chains approach their maximal extensibility.

In summary, under conditions of low viscoelasticity, fracture propagation is limited as discussed above, by the propagation of a crack in the matrix network, leading to a threshold amount of filler network bond scission before propagation can occur

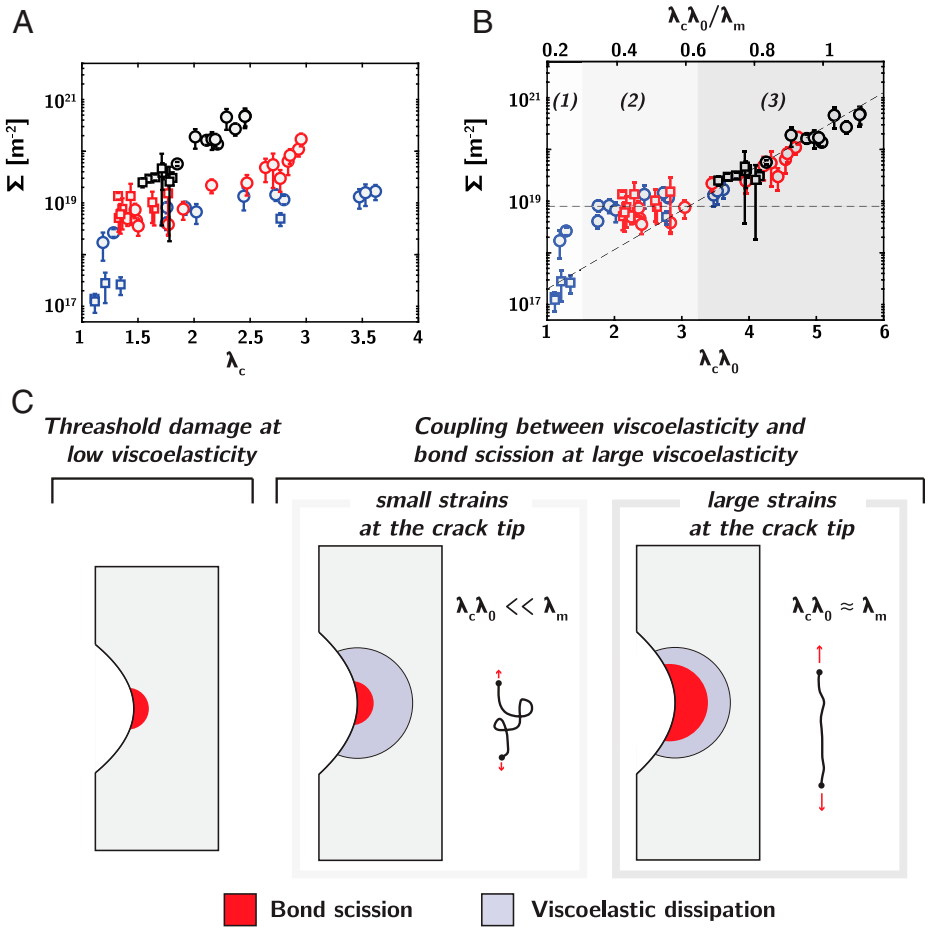

Fig. 6. Coupling of chain scission with viscoelastic dissipation and macroscopic deformation. (*A*) Areal density of broken chains Σ as a function of strain at break λ_c, giving an estimation of the relative damage zone width during propagation. (*B*) Areal density of broken chains Σ as a function of the effective filler network strain at break $\lambda_c\lambda_0$. (*C*) Schematic illustrating the coupling of bond scission with macroscopic deformation. At low viscoelasticity, bond scission reaches a threshold value associated with damage percolation in the filler network (regime 1). At high viscoelasticity, two regimes can be observed, depending on the effective stretch on the filler network. When this effective stretch $\lambda_c\lambda_0$ is much smaller than the limiting extensibility λ_m, bond scission and viscoelastic dissipation are decoupled, leading to a purely additive contribution (regime 2). In the limit where $\lambda_c\lambda_0 \approx \lambda_m$, additional bond scission occurs due to coupling with the macroscopic deformation field in the material (regime 3).

(Fig. 4*B* and 5*B*). This threshold level is highly dependent on the network prestretch and controls also the threshold fracture energy.

For each material, increasing viscoelasticity leads to an increase in the bulk strain at break λ_c and the strains at the crack tip. However, the situation differs for the three types of network.

In single networks, chain rupture leads to direct localization, correlated bond scission, and catastrophic failure (Fig. 5*A*), and most probably there is no well-defined softened zone. In this case, viscoelasticity increases the required energy release rate to propagate the crack at a certain speed and increased bond scission is a consequence of the higher crack tip strains (22). Because of this localization of rupture, no mechanism prevents the crack from moving even very slowly and threshold values of Σ/Σ_{LT} and $\Gamma_c^{\lambda_0,*}$ are very low.

In MNE, when the effective bulk strain at break on the filler network remains small compared to its limiting extensibility, i.e., $\lambda_0\lambda_c < 0.6\,\lambda_{max}$, the material forms a highly damaged zone at the crack tip. In this regime, fracture energy can then be simply expressed as the sum of a constant contribution due to bond scission at the damage percolation threshold and a strain rate-dependent viscoelastic contribution (Fig. 6*C*, $\lambda_0\lambda_c \ll \lambda_m$). If the effective strains on the filler network become larger, i.e., $\lambda_0\lambda_c > 0.6\,\lambda_{max}$, the local probability of bond scission at the crack tip increases strongly, leading to an increase in the overall amount of bond scission Σ/Σ_{SN} for increasing viscoelasticity and increasing strains (Fig. 6*C*, $\lambda_0\lambda_c \approx \lambda_m$). However, the increase in sacrificial bond scission in this second regime appears more as a consequence of the increase in viscoelastic dissipation through the increase in local strains at the crack tip, rather than the cause for the reinforcement of the network when increasing viscoelasticity. Indeed, as evidenced in Fig. 2*D*, no such cross-over is observed when plotting the normalized fracture energy $\Gamma_c\lambda_0^2$ as a function of the effective strain $\lambda_c\lambda_0$.

Variation of threshold fracture energy with prestretch. These observations pose the question of the existence of an optimal value of initial prestretch of the filler network to toughen the elastomer in the threshold regime at low viscoelasticity. In particular, when the strands of the filler network are close to their limiting extensibility already under static conditions, one may ask whether such a sacrificial network can still effectively delay crack propagation through the mechanism described in Fig. 5.

Fig. 7 shows the threshold fracture energy $\Gamma_c^{\lambda_0,*}$ as a function of prestretch for a series of PEA-based MNE (details of synthesis and mechanical properties in *SI Appendix*, Fig. S5 and ref. 7). Given the value of T_g at −18 °C, this situation is close to threshold conditions. Although no damage data are available

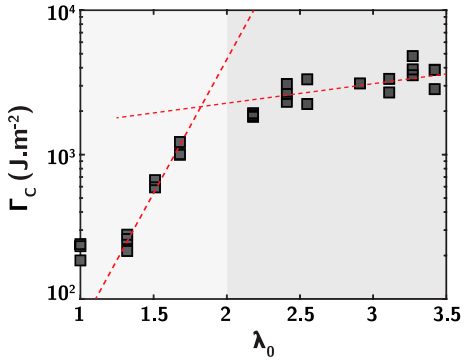

Fig. 7. Variation of the fracture energy as a function of degree of prestretch. Results are obtained for solvent-synthetized PEA materials, fractured close to threshold conditions, at stretch rate $\dot{\lambda} = 4 \times 10^{-3}$ s^{-1} and temperature $T = 25$°C. Red dashed lines and gray areas highlight two successive regimes of , respective strong and weak increases of Γ_c with λ_0.

for this series, it is clear that there appears to be a threshold prestretch $\lambda_0 \approx 2$, above which Γ_c increases more slowly.

Following Fig. 5, the creation of the energy dissipating damage zone is due to the delay in correlated bond breakage which initially increases with dilution as seen in the first regime of Fig. 7, for $\lambda_0 \leq 2$. However, when the filler network becomes close to its maximum stretch ($\lambda_0 \geq 2$), the transition from regime *i* to *ii* and *ii* to *iii* must occur at increasingly lower values of macroscopic stretch, which causes the saturation observed in Fig. 7.

This saturation is here observed at $\lambda_0 \approx 2$, for which the effective critical stretch at break on the filler network is $\lambda_0 \lambda_c \approx 3.3$, approaching its limiting extensibility $\lambda_{\text{limit}} = 5.1$ (*SI Appendix*, Fig. S7) (7).

Conclusion. We have simultaneously quantified the fracture energy and the extent of molecular damage occurring near the fracture surfaces in a series of prenotched multiple network elastomers tested at different stretch rates and temperatures. We find that while bond scission and viscoelastic dissipation are roughly proportional to each other in simple networks, the introduction of a prestretched sacrificial network creates a clear threshold level of bond scission for the crack to propagate that is still active in the absence of viscoelastic dissipation. This threshold value of bond scission necessary for crack propagation in MNE increases with prestretch λ_0 and has an almost two orders of magnitude toughening effect at $T \gg T_g$ where viscoelastic dissipation is minimal.

We showed with mechanochemistry that the large increase in the threshold Γ_c for MNE is correlated to the existence of a large damage zone (over hundreds of network mesh sizes) ahead of the propagating crack, where filler network bonds break. We propose that bond scission in MNE occurs in three stages as described in Fig. 5: (*i*) mean-field bond scission of the filler network far from the crack tip, (*ii*) correlated bond scission of the filler network closer to the tip leading to increased stretchability of this highly damaged zone, and (*iii*) localized scission of the matrix bonds in this highly damaged region, conducting to crack propagation. The existence of a large minimum size of the damage zone in MNE is due to a rate-independent mechanism of stress delocalization that delays the correlated bond scission needed to grow a crack.

The values of the local stretch λ where the transition between these mechanisms is observed vary with network structure and decrease with filler network prestretch λ_0. There is however a hard limit to the accessible filler network prestretch given by the average chain length between cross-links, above which correlated filler network damage (*ii*) and matrix failure (*iii*) may occur at too close values of stretch, leading to a saturation of Γ_c with increasing λ_0.

This mechanism of stress delocalization introduces a threshold for crack nucleation that effectively protects elastomers from crack propagation even at a high temperature. This threshold damage remains active at lower temperatures, where viscoelastic dissipation additionally contributes to toughness. These results may have important implications on the design of intrinsically tough elastomers. In conventionally filled elastomers where nanoparticle fillers may play a role of sacrificial network, highly fractal fillers that form a network at low volume fraction may be intrinsically more effective at delaying crack nucleation, a mechanism which could become more important at high temperature.

Materials and Methods

Sacrificial filler networks are synthesized from a solution of monomer, cross-linker, mechanophore cross-linker, and ultraviolet (UV) initiator. In these networks, 5% of the cross-linkers are replaced by a mechanosensitive DACL. These networks are then swollen to equilibrium in a bath of methyl acrylate or ethyl acrylate monomers and cross-linker, which are subsequently UV polymerized. These swelling and polymerization steps can be repeated several times to obtain double and triple networks, respectively. Details are described in *SI Appendix*, section SI.1. Uniaxial tensile tests of unnotched and notched samples were carried out on an Instron 5565 tensile testing machine at a constant stretch rate, and details on the experimental set-up for mechanical measurements and measurement of the fracture energy and crack propagation speed are described in *SI Appendix*, section SI.2. The characterization of the areal chain density of the filler network in multiple networks was estimated from the analysis of the stress-strain curves and the analysis method is described in *SI Appendix*, section SI.3. The series of polyethyl acrylates was synthesized in the presence of solvent that was eventually evaporated. Details of the composition and mechanical properties are shown in *SI Appendix*, section SI.4. Finally, we present in *SI Appendix*, section SI.5, the confocal set-up and the quantitative image analysis (following image collection, vignetting and flatfield correction, and calibration of fluorescence intensity) and we discuss the bulk activation in TN.DA.MA.MA samples and the analysis of bifurcations and inhomogeneous crack front in DA.DN.EA.EA.

Data Availability. All study data are included in the article and/or *SI Appendix*.

ACKNOWLEDGMENTS. We gratefully acknowledge the advice of Robert Goestl (RWTH Aachen) and Christophe Meyer (ESPCI) on the synthesis of the mechanophore and helpful discussions with Gabriel Sanoja (Current address: Department of Chemical Engineering, University of Texas Austin, Austin, TX). This project has received funding from the European Research Council (ERC) under the European Union's Horizon 2020 research and innovation program under grant agreement AdG no. 695351.

1. T. L. Smith, Dependence of the ultimate properties of a GR-S rubber on strain rate and temperature. *J. Polym. Sci.* **32**, 99–113 (1958).
2. C. Creton, M. Ciccotti, Fracture and adhesion of soft materials: A review. *Rep. Prog. Phys.* **79**, 046601 (2016).
3. D. De, A. N. Gent, Tear strength of carbon-black-filled compounds. *Rubber Chem. Technol.* **69**, 834–850 (1996).
4. H. Zhang *et al.*, Nanocavitation around a crack tip in a soft nanocomposite: A scanning microbeam small angle X-ray scattering study. *J. Polym. Sci., B, Polym. Phys.* **53**, 422–429 (2015).
5. J. P. Gong, Y. Katsuyama, T. Kurokawa, Y. Osada, Double-network hydrogels with extremely high mechanical strength. *Adv. Mater.* **15**, 1155–1158 (2003).
6. E. Ducrot, Y. Chen, M. Bulters, R. P. Sijbesma, C. Creton, Toughening elastomers with sacrificial bonds and watching them break. *Science* **344**, 186–189 (2014).
7. P. Millereau *et al.*, Mechanics of elastomeric molecular composites. *Proc. Natl. Acad. Sci. U.S.A.* **115**, 9110–9115 (2018).
8. R. E. Webber, C. Creton, H. R. Brown, J. P. Gong, Large strain hysteresis and Mullins effect of tough double-network hydrogels. *Macromolecules* **40**, 2919–2927 (2007).
9. T. Matsuda *et al.*, Yielding criteria of double network hydrogels. *Macromolecules* **49**, 1865–1872 (2016).

10. T. Matsuda, R. Kawakami, T. Nakajima, J. P. Gong, Crack tip field of a double-network gel: Visualization of covalent bond scission through mechanoradical polymerization. *Macromolecules* **53**, 8787–8795 (2020).
11. Q. M. Yu, Y. Tanaka, H. Furukawa, T. Kurokawa, J. P. Gong, Direct observation of damage zone around crack tips in double-network gels. *Macromolecules* **42**, 3852–3855 (2009).
12. H. R. Brown, A model of the fracture of double network gels. *Macromolecules* **40**, 3815–3818 (2007).
13. Y. Tanaka, A local damage model for anomalous high toughness of double-network gels. *EPL* **78**, 56005 (2007).
14. Y. Tanaka *et al.*, Localized yielding around crack tips of double-network gels. *Macromol. Rapid Commun.* **29**, 1514–1520 (2008).
15. Y. Chen, G. Sanoja, C. Creton, Mechanochemistry unveils stress transfer during sacrificial bond fracture of tough multiple network elastomers. *Chem. Sci. (Camb.)* **12**, 11098–11108 (2021).
16. Y. Tanaka *et al.*, Determination of fracture energy of high strength double network hydrogels. *J. Phys. Chem. B* **109**, 11559–11562 (2005).
17. I. Kolvin, J. M. Kolinski, J. P. Gong, J. Fineberg, How supertough gels break. *Phys. Rev. Lett.* **121**, 135501 (2018).
18. X. P. Morelle *et al.*, Highly stretchable and tough hydrogels below water freezing temperature. *Adv. Mater.* **30**, e1801541 (2018).
19. A. N. Gent, Adhesion and strength of viscoelastic solids. Is there a relationship between adhesion and bulk properties? *Langmuir* **12**, 4492–4495 (1996).
20. B. N. J. Persson, O. Albohr, G. Heinrich, H. Ueba, Crack propagation in rubber-like materials. *J. Phys. Condens. Matter* **17**, R1071 (2005).
21. P. G. De Gennes, Soft adhesives. *Langmuir* **12**, 4497–4500 (1996).
22. J. Slootman *et al.*, Quantifying rate-and temperature-dependent molecular damage in elastomer fracture. *Phys. Rev. X* **10**, 41045 (2020).
23. W. Qiu, P. A. Gurr, G. G. Qiao, Regulating color activation energy of mechanophore-linked multinetwork elastomers. *Macromolecules* **53**, 4090–4098 (2020).
24. Y. Chen, C. J. Yeh, Y. Qi, R. Long, C. Creton, From force-responsive molecules to quantifying and mapping stresses in soft materials. *Sci. Adv.* **6**, eaaz5093 (2020).
25. H. W. Greensmith, Rupture of rubber. X. The change in stored energy on making a small cut in a test piece held in simple extension. *J. Appl. Polym. Sci.* **7**, 993–1002 (1963).
26. T. L. Smith, Ultimate tensile properties of elastomers. I. Characterization by a time and temperature independent failure envelope. *J. Polym. Sci. A* **1**, 3597–3615 (1963).
27. P.-G. de Gennes, "Fracture d'un adhésif faiblement réticulé" in *Simple Views on Condensed Matter* (World Scientific, 2003), pp. 431–436.
28. B. N. J. Persson, E. A. Brener, Crack propagation in viscoelastic solids. *Phys. Rev. E Stat. Nonlin. Soft Matter Phys.* **71** (3 Pt 2A), 036123 (2005).
29. S. Wang, S. Panyukov, M. Rubinstein, S. L. Craig, Quantitative adjustment to the molecular energy parameter in the Lake-Thomas theory of polymer fracture energy. *Macromolecules* **52**, 2772–2777 (2019).
30. H. J. Hermann, S. Roux, "Modelization of fracture in disordered systems" in *Statistical Models for the Fracture of Disordered Media*, H. J. Hermann, S. Roux, Eds. (Random Materials and Processes, Elsevier, 2014), pp. 159–188.
31. S. Pradhan, B. K. Chakrabarti, A. Hansen, Crossover behavior in a mixed-mode fiber bundle model. *Phys. Rev. E Stat. Nonlin. Soft Matter Phys.* **71** (3 Pt 2A), 036149 (2005).
32. G. Lake, A. Thomas, The strength of highly elastic materials. *Proc. R. Soc. London. Ser. A. Math. Phys. Sci.* **300**, 108–119 (1967).
33. S. R. Lavoie, P. Millereau, C. Creton, R. Long, T. Tang, A continuum model for progressive damage in tough multinetwork elastomers. *J. Mech. Phys. Solids* **125**, 523–549 (2019).
34. M. Bacca, C. Creton, R. M. McMeeking, A model for the Mullins effect in multinetwork elastomers. *J. Appl. Mech. Trans. ASME* **84**, 121009 (2017).
35. H. R. Brown, A molecular interpretation of the toughness of glassy polymers. *Macromolecules* **24**, 2752–2756 (1991).
36. C. Y. Hui, A. Ruina, C. Creton, E. J. Kramer, Micromechanics of crack growth into a craze in a polymer glass. *Macromolecules* **25**, 3948–3955 (1992).
37. J. Tauber, S. Dussi, J. Van Der Gucht, Microscopic insights into the failure of elastic double networks. *Phys. Rev. Mater.* **4**, 1–12 (2020).
38. J. Tauber, L. Rovigatti, S. Dussi, J. van der Gucht, Sharing the load: Stress redistribution governs fracture of polymer double networks. *Macromolecules* **54**, 8563–8574 (2021).